ChemComm

COMMUNICATION

View Article Online
View Journal | View Issue

Cite this: *Chem. Commun.*, 2014, **50**, 1652

Received 14th October 2013,
Accepted 9th December 2013

DOI: 10.1039/c3cc47885h

www.rsc.org/chemcomm

The effect of a macrocyclic constraint on electron transfer in helical peptides: A step towards tunable molecular wires†

Jingxian Yu,*[a] John R. Horsley,[a] Katherine E. Moore,[b] Joe G . Shapter[b] and Andrew D. Abell*[a]

Two helical peptides, one constrained by a covalent side-chain staple, exhibit vastly different electronic properties despite adopting essentially the same backbone conformation. High level calculations confirm that these differences are due to the additional backbone rigidity imparted by the macrocyclic constraint.

Helical domains in peptides and proteins provide a good medium for electron transfer[1–5] over surprisingly long molecular distances (>100 Å).[6] Such structures present as ideal candidates for use as molecular wires, particularly when combined with an ability to be precisely functionalised.[7–9] However, more detailed understanding of exactly what defines and controls the mechanisms and efficiency of electron transfer in peptides is required before this promise can be fully realised. Toward this goal, we recently demonstrated that intramolecular hydrogen bonding within helical Aib (α-aminoisobutyric acid) containing oligomers plays a critical role in defining the mechanism of electron transfer.[10,11] Recent theoretical studies suggest that low-frequency rotation between neighbouring amino acids brings adjacent carbonyl groups into alignment to allow efficient charge transfer through the peptide.[12,13] As such any feature that enhances backbone rigidity should restrict molecular motion and consequently retard electron transfer in peptides. However, the exact influence of backbone rigidity on electron transfer requires significant further investigation.[14–17] Here we present electrochemical and theoretical studies on a helical peptide constrained by a side-chain tether to begin to unravel these effects in isolation from other factors such as chain length, dipole orientation and the associated hydrogen bonding that are known to influence electron transfer.

The required Aib-rich hexapeptide stapled with an i to $i + 3$ macrocyclic constraint by Huisgen cycloaddition (peptide **1**) and a linear analog (peptide **2**) were synthesised as described in ESI.† The peptides were designed to share a common 3_{10}-helical backbone conformation, with peptide **1** possessing a rigid backbone conformation as defined by the side-chain constraint (Scheme 1).

The geometries of peptides **1** and **2** were confirmed as 3_{10}-helical by ^{1}H NMR spectroscopy. In particular, NH (i) to NH ($i + 1$) ROESY correlations were observed for both peptides and also their synthetic precursors, **3–5** and **6** and **7**. Furthermore, C$^\alpha$H (i) to NH ($i + 1$) and medium range C$^\alpha$H (i) to NH ($i + 2$) were found for **1** and **2**, with long range C$^\alpha$H (i) to NH ($i + 3$) correlations evident in peptides **3**, **5** and **7**, as detailed in the ESI.† A lack of C$^\alpha$H (i) to NH ($i + 4$) correlations for all peptides precludes the possibility of an α-helical structure, which is characterised by (i to $i + 4$) hydrogen bonds.[18] A strong negative minimum near 202 nm, with a far weaker minimum at approximately 232 nm was observed in a representative CD spectrum of the constrained peptide **3** (see ESI†), which further supports a 3_{10}-helical conformation.[19,20] Collectively, this information confirms the presence of a 3_{10}-helical backbone structure and that the C-terminal ferrocene and the constraint do not impinge on the backbone helicity.

The lowest energy conformers for the *N*-protected peptides **5** and **7** were determined by molecular modelling (using a hybrid B3LYP method with the 6-31G** basis set for all C, H, N, O atoms,

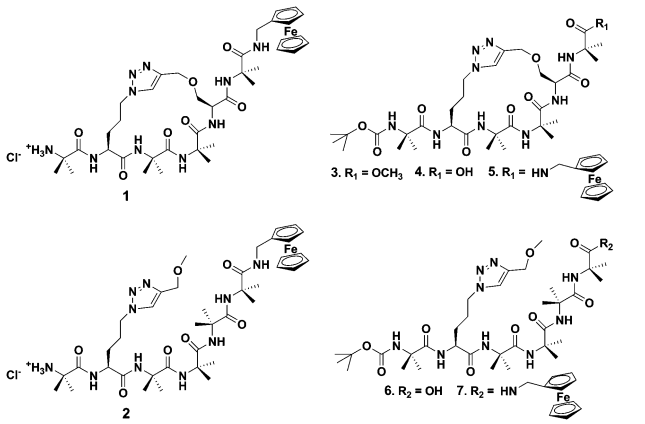

Scheme 1 Structures of target peptides **1** and **2** and key synthetic intermediates.

[a] *School of Chemistry and Physics, The University of Adelaide, Adelaide, SA 5005, Australia. E-mail: jingxian.yu@adelaide.edu.au, andrew.abell@adelaide.edu.au*
[b] *School of Chemical & Physical Sciences, Flinders University, Bedford Park, SA 5042, Australia*

† Electronic supplementary information (ESI) available. See DOI: 10.1039/c3cc47885h

and the Lanl2dz basis set for Fe atoms) in order to further define the backbone conformations of the constrained and unconstrained peptides. The *N*-protected peptides were used in these studies as free amines are known to give rise to unrealistic electrostatic interactions, resulting in unstable lowest energy conformers.[21] The resulting structures (see ESI†) reveal that the distances from the first to last carbonyl carbons (backbone lengths) of the two peptides are similar, 11.94 Å and 12.02 Å for peptides **5** and **7** respectively. In addition, the greatest variation between hydrogen bond lengths is 0.14 Å. The mean dihedral angles for residues 1–4 of peptide **5** were calculated to be −56.86° for Ø and −31.29° for Ψ, deviating from an ideal 3_{10}-helix by 0.14° and 1.29°, respectively,[22] whilst the mean dihedral angles for residues 1–4 deviated from an ideal 3_{10}-helix by 1.33° and 3.75° in peptide **7**. These studies demonstrate that the two structures have essentially the same conformations, such that they differ only in the presence (or absence) of the constraint and the associated effect that this has on backbone rigidity.

The constrained peptide **1** and linear analog **2** were next separately attached to vertically aligned single-walled carbon nanotube array/gold (SWCNTs/Au) electrodes[23,24] (see ESI† for details) in order to study their electron transfer kinetics. SWCNTs/Au electrodes provide a high surface concentration of attached redox probes and hence high sensitivity and reproducibility of electrochemical measurement.[25–27] Fig. 1 shows the cyclic voltammograms obtained for the two target peptides immersed in 0.1 mol L^{-1} $TBAPF_6$–CH_3CN solutions. These show a pair of redox peaks, characteristic of a one-electron oxidation–reduction reaction (Fc^+/Fc). The surface concentrations of the peptides were determined by integrating background current subtracted peak areas to be 3.76×10^{-10} mol cm^{-2} for **1** and 2.52×10^{-10} mol cm^{-2} for **2** (see Table 1). These surface concentrations are comparable to other carbon nanotube electrode studies.[10,23] The formal potentials (E_o) and apparent electron transfer rate constants (k_{app}) were estimated to be 0.853 V and 28.1 s^{-1} for **1** and 0.371 V and 117.3 s^{-1} for **2**, respectively (as detailed in Table 1), using Laviron's formalism.[28]

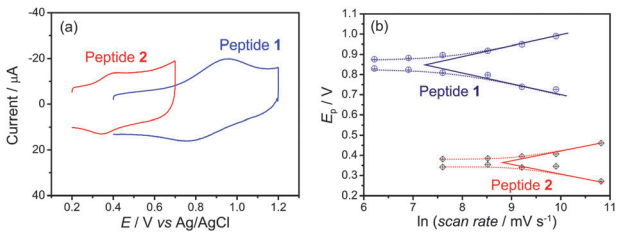

Fig. 1 (a) Cyclic voltammograms of peptide **1** (blue) and peptide **2** (red) immobilised on SWCNTs/Au electrodes taken at 5 V s^{-1}. (b) Peak potential *versus* ln(scan rate) for peptides **1** and **2** after background current subtraction.

Table 1 Electron transfer rate constants (k_{app}), surface concentrations and formal potentials (E_o) of the constrained peptide (peptide **1**) and linear analog (peptide **2**)

Peptide	Surface concentration ($\times 10^{-10}$ mol cm^{-2})	E_o (V *vs.* AgCl/Ag)	k_{app} (s^{-1})
1	3.76 ± 0.35	0.853	28.1 ± 3.6
2	2.52 ± 0.18	0.371	117.3 ± 9.9

Despite having very similar backbone geometries, the two target peptides exhibit considerably different formal potentials and electron transfer rate constants. Side-bridge stapling as in peptide **1** results in a significant formal potential shift to the positive of approximately 480 mV in comparison to peptide **2**. Thus oxidation–reduction of the redox-active ferrocene moiety in the constrained peptide is energetically much less favourable than in the linear analog. Such a dramatic formal potential shift has not, to the best of our knowledge, been previously reported in ferrocene-derivatised peptides. As both peptides essentially differ only in the presence (or absence) of the side-bridge constraint, the significant formal potential shift found in **1** is clearly a result of additional backbone rigidity imparted by this constraint. Our experimental data also reveal a significant decrease in the electron transfer rate constant (approx. 25%) upon introducing the constraint of **1**. Previous studies have shown that electron transfer rate constants in peptides can vary greatly,[6,10,17] but without such a significant difference in formal potential as reported here. Our results suggest that side-bridge stapling creates an additional reorganisation energy barrier that impedes electron transfer within the peptide, in turn decreasing the charge transfer rate. Hence reducing the backbone flexibility within a helical peptide through the introduction of a constraint lowers the rate of electron transfer by restricting the precise torsional motions that lead to facile intramolecular electron transfer along the backbone. Thus side-bridge stapling provides a unique approach to manipulate energy barriers and conductance in peptides.

Interestingly, the all Aib containing linear peptide **8** (see ESI†) gave a formal potential shift to the positive of 137 mV and approximate two-fold decrease in the electron transfer rate constant compared to **2**. This peptide adopts essentially the same backbone conformation as the earlier peptides based on NMR and modelling studies as discussed in the ESI.† However, it would be expected to have somewhat reduced backbone flexibility relative to **2** with the inclusion of an additional geminally disubstituted residue. The electrochemical data are consistent with this notion, where the electron transfer rate constant is intermediary between that of the constrained peptide **1** and its linear analog **2**. This observation further supports the link between backbone flexibility and the rate of electron transfer, as has also been noted for DNA and PNA.[29,30]

Theoretical calculations, using the latest constrained density functional theory (cDFT),[31] were performed on the model peptides **9** and **10** (see Fig. 2) in order to corroborate our experimental observations. These peptides were chosen for this study since they contain the same sequence as **1** and **2**, but with ferrocene units at both termini to act as both a donor and an acceptor. Calculation of reorganisation energies for electron transfer along the backbone then provides an insight into the intramolecular electron transfer dynamics. Diabatic states were constructed by individually localising an overall charge of 1 on each of the ferrocene units and amino acids, as shown in Fig. 2. Diabatic potential profiles were determined by assuming that during an electron hopping step, the nuclear configuration changes smoothly between the optimised geometries of the diabatic states in which the excess charge is localised before and after electron transfer[32] (see ESI†). Peptides **9** and **10** show comparable reorganisation

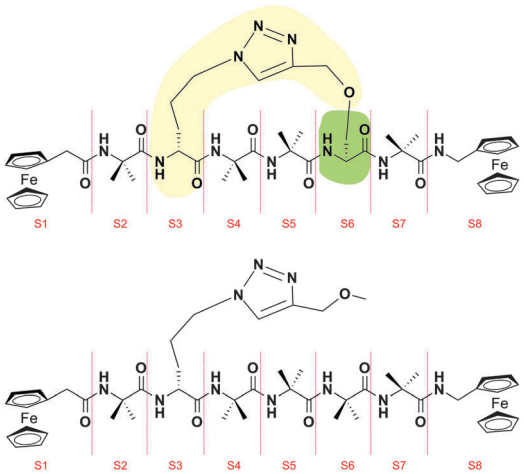

Fig. 2 Constructed diabatic states in constrained peptide **9** (top) and unconstrained peptide **10** (bottom). Charge localisation fragments of the molecule involving the side bridge are indicated using two different colours in peptide **9**.

Table 2 Comparison of computed reorganisation energies for electron hopping steps involving diabatic state S3 in the two model peptides (**9** and **10**)

Hopping step	Peptide **9** (kcal mol^{-1})	Peptide **10** (kcal mol^{-1})	Difference (kcal mol^{-1})
S2 → S3	28.99	24.09	4.90
S3 → S2	30.62	24.57	6.05
S3 → S4	25.41	22.27	3.14
S4 → S3	30.68	23.71	6.97

energies for all electron hopping steps, except those involving diabatic state S3. The reorganisation energies for the forward and backward electron hopping steps from diabatic state S3 in **9** are much higher than those for the corresponding steps in **10** (see Table 2). The introduction of the side-bridge gives rise to a significant increase in reorganisation energy, in the range of 3.14–6.97 kcal mol^{-1}. Thus the higher reorganisation energy barrier in peptide **9** is a direct result of the side-bridge constraint, thus further supporting our experimental results.

In summary, electrochemical studies are reported on two peptides containing Aib residues that constrain the backbones into a well-defined 3_{10}-helix, a secondary structure known to favour electron transfer. The first of these peptides (**1**) has its helical geometry stabilised with a covalent constraint that links its i and $i + 3$ side chains, resulting in additional conformational rigidity in the backbone. Electrochemical studies revealed that peptide **1** exhibited a significant formal potential shift to the positive (480 mV), and a substantial decrease in the electron transfer rate constant (25%), compared to the unconstrained peptide **2**. These differences reflect the extent of backbone rigidity imparted by the side-bridge constraint. In support, the all Aib containing linear peptide **8** displayed formal potential and electron transfer rate constant values between those of peptides **1** and **2**. This reflects an intermediary backbone rigidity for this peptide. High level calculations confirm that the additional reorganisation energy barrier is a direct result of the backbone rigidity imparted by the side-bridge constraint. Thus the tether significantly impedes intramolecular electron transfer by enhancing the rigidity of the peptide backbone. This then generates an additional reorganisation energy barrier which restricts the necessary torsional motions that lead to facile intramolecular electron transfer along the backbone. Our results provide definitive evidence of a direct link between backbone rigidity and electron transfer in peptides. These findings provide a new means to fine tune the rates of electron transfer in peptides, which represent an important step towards their implementation into molecular electronic assemblies.

Notes and references

1 H. S. Mandal and H.-B. Kraatz, *J. Phys. Chem. Lett.*, 2012, **3**, 709.
2 R. A. Malak, Z. N. Gao, J. F. Wishart and S. S. Isied, *J. Am. Chem. Soc.*, 2004, **126**, 13888.
3 P. A. Brooksby, K. H. Anderson, A. J. Downard and A. D. Abell, *J. Phys. Chem. C*, 2011, **115**, 7516.
4 J. Yu, D. M. Huang, J. G. Shapter and A. D. Abell, *J. Phys. Chem. C*, 2012, **116**, 26608.
5 Y.-F. Wang, Z.-Y. Yu, J. Wu and C.-B. Liu, *J. Phys. Chem. A*, 2009, **113**, 10521–10526.
6 Y. Arikuma, H. Nakayama, T. Morita and S. Kimura, *Angew. Chem., Int. Ed.*, 2010, **49**, 1800.
7 J. A. Gao, P. Muller, M. Wang, S. Eckhardt, M. Lauz, K. M. Fromm and B. Giese, *Angew. Chem., Int. Ed.*, 2011, **50**, 1926.
8 J. Watanabe, T. Morita and S. Kimura, *J. Phys. Chem. B*, 2005, **109**, 14416.
9 M. Lauz, S. Eckhardt, K. M. Fromm and B. Giese, *Phys. Chem. Chem. Phys.*, 2012, **14**, 13785–13788.
10 J. Yu, O. Zvarec, D. M. Huang, M. A. Bissett, D. B. Scanlon, J. G. Shapter and A. D. Abell, *Chem. Commun.*, 2012, **48**, 1132.
11 J. Yu, J. R. Horsley and A. D. Abell, *Aust. J. Chem.*, 2013, **66**, 848.
12 E. W. Schlag, S. Y. Sheu, D. Y. Yang, H. L. Selzle and S. H. Lin, *Proc. Natl. Acad. Sci. U. S. A.*, 2000, **97**, 1068.
13 E. W. Schlag, S. Y. Sheu, D. Y. Yang, H. L. Selzle and S. H. Lin, *Angew. Chem., Int. Ed.*, 2007, **46**, 3196.
14 S. Okamoto, T. Morita and S. Kimura, *Langmuir*, 2009, **25**, 3297.
15 G. A. Orlowski, S. Chowdhury and H. B. Kraatz, *Electrochim. Acta*, 2007, **53**, 2034.
16 K. Takeda, T. Morita and S. Kimura, *J. Phys. Chem. B*, 2008, **112**, 12840.
17 M. M. Galka and H. B. Kraatz, *ChemPhysChem*, 2002, **3**, 356.
18 Z. Biron, S. Khare, A. O. Samson, Y. Hayek, F. Naider and J. Anglister, *Biochemistry*, 2002, **41**, 12687.
19 C. Toniolo, A. Polese, F. Formaggio, M. Crisma and J. Kamphuis, *J. Am. Chem. Soc.*, 1996, **118**, 2744.
20 A. K. Boal, I. Guryanov, A. Moretto, M. Crisma, E. L. Lanni, C. Toniolo, R. H. Grubbs and D. J. O'Leary, *J. Am. Chem. Soc.*, 2007, **129**, 6986.
21 N. A. Burton, M. J. Harrison, J. C. Hart, I. H. Hillier and D. W. Sheppard, *Faraday Discuss. Chem. Soc.*, 1998, **110**, 463.
22 O. Jacobsen, H. Maekawa, N. H. Ge, C. H. Gorbitz, P. Rongved, O. P. Ottersen, M. Amiry-Moghaddam and J. Klaveness, *J. Org. Chem.*, 2011, **76**, 1228.
23 J. J. Gooding, R. Wibowo, J. Q. Liu, W. R. Yang, D. Losic, S. Orbons, F. J. Mearns, J. G. Shapter and D. B. Hibbert, *J. Am. Chem. Soc.*, 2003, **125**, 9006.
24 K. E. Moore, B. S. Flavel, A. V. Ellis and J. G. Shapter, *Carbon*, 2011, **49**, 2639.
25 K. E. Moore, B. S. Flavel, J. Yu, A. D. Abell and J. G. Shapter, *Electrochim. Acta*, 2013, **89**, 206.
26 K. T. Constantopoulos, C. J. Shearer, A. V. Ellis, N. H. Voelcker and J. C. Shapter, *Adv. Mater*, 2010, **22**, 557.
27 P. Diao and Z. F. Liu, *Adv. Mater.*, 2010, **22**, 1430.
28 E. Laviron, *J. Electroanal. Chem.*, 1979, **100**, 263.
29 E. Wierzbinski, A. de Leon, X. Yin, A. Balaeff, K. L. Davis, S. Reppireddy, R. Venkatramani, S. Keinan, D. H. Ly, M. Madrid, D. N. Beratan, C. Achim and D. H. Waldeck, *J. Am. Chem. Soc.*, 2012, **134**, 9335.
30 E. Hatcher, A. Balaeff, S. Keinan, R. Venkatramani and D. N. Beratan, *J. Am. Chem. Soc.*, 2008, **130**, 11752.
31 T. Van Voorhis, T. Kowalczyk, B. Kaduk, L. P. Wang, C. L. Cheng and Q. Wu, *Annu. Rev. Phys. Chem.*, 2010, **61**, 149–170.
32 A. Farazdel, M. Dupuis, E. Clementi and A. Aviram, *J. Am. Chem. Soc.*, 1990, **112**, 4206.

